International Journal of Pharmaceutics 526 (2017) 1–10

International Journal of Pharmaceutics

journal homepage: www.elsevier.com/locate/ijpharm

Mathematical modelling of liquid transport in swelling pharmaceutical immediate release tablets

Daniel Markl[a], Samy Yassin[a], D. Ian Wilson[a], Daniel J. Goodwin[b], Andrew Anderson[b], J. Axel Zeitler[a,*]

[a] Department of Chemical Engineering and Biotechnology, University of Cambridge, West Cambridge Site, Philippa Fawcett Drive, Cambridge CB3 0AS, UK
[b] GlaxoSmithKline, New Frontiers Science Park, Harlow, Essex CM19 5AW, UK

ARTICLE INFO

Article history:
Received 30 January 2017
Received in revised form 8 March 2017
Accepted 6 April 2017
Available online 8 April 2017

Keywords:
Powder compacts
Tablet disintegration
Terahertz pulsed imaging
Liquid penetration
Swelling
Porosity

ABSTRACT

Oral dosage forms are an integral part of modern health care and account for the majority of drug delivery systems. Traditionally the analysis of the dissolution behaviour of a dosage form is used as the key parameter to assess the performance of a drug product. However, understanding the mechanisms of disintegration is of critical importance to improve the quality of drug delivery systems. The disintegration performance is primarily impacted by the hydration and subsequent swelling of the powder compact. Here we compare liquid ingress and swelling data obtained using terahertz pulsed imaging (TPI) to a set of mathematical models. The interlink between hydration kinetics and swelling is described by a model based on Darcy's law and a modified swelling model based on that of Schott. Our new model includes the evolution of porosity, pore size and permeability as a function of hydration time. Results obtained from two sets of samples prepared from pure micro-crystalline cellulose (MCC) indicate a clear difference in hydration and swelling for samples of different porosities and particle sizes, which are captured by the model. Coupling a novel imaging technique, such as TPI, and mathematical models allows better understanding of hydration and swelling and eventually tablet disintegration.

1. Introduction

Oral dosage forms, such as tablets, are one of the most widely used drug delivery systems for treating patients today. There are strict regulations on how these tablets should perform: immediate release formulations should release their entire active pharmaceutical ingredient (API) within 10 min of ingestion (Gupta et al., 2006; Battu et al., 2007; Corveleyn and Remon, 1997), while for sustained release tablet formulations the requirement is to release their full API content within 24 h (Davis et al., 1986). Furthermore, generics manufacturers have to pass bio-equivalency studies with respect to the original products on which the generic product is based (Sarantopoulos et al., 1995). Two key pre-requisites are required to achieve this: (1) a comprehensive understanding of the excipients used and how they will affect tablet disintegration as well as dissolution; and (2) reliable and accurate analytical techniques for assessing tablet dissolution, disintegration and API release and the underlying mechanisms (Lin, 1988; Yu, 2008). Progress has been made experimentally to understand hydration phenomena and API release kinetics observed in tablets and thus relate them to the choice of excipient and resulting tablet microstructure using destructive (Segale et al., 2010) and non-destructive analytical techniques (Battu et al., 2007; Bi et al., 1999; Chen et al., 2010; Kazarian and van der Weerd, 2008; Kazarian and Chan, 2006; Rajabi-Siahboomi et al., 1996).

Magnetic resonance imaging (MRI) has been used extensively to investigate the hydration and swelling processes in sustained released formulations (Chen et al., 2010; Fyfe and Blazek, 1997; Rajabi-Siahboomi et al., 1996, 1994). For example MRI has shown that multiple phases of hydration co-exist in hydroxypropylmethylcellulose (HPMC) compacts: viz. a dry phase at the core of the tablet, followed by a glassy phase, a swollen glassy phase and finally a gel phase in direct contact with the dissolution medium (Chen et al., 2010; Zhang et al., 2011, 2013). More recently it was shown that terahertz pulsed imaging (TPI) can be used to measure the liquid ingress and the swelling of rapid disintegrating tablets simultaneously (Yassin et al., 2015a).

Alongside the need for good analytical techniques to assess the tablet performance, there is a need for theoretical models predicting tablet disintegration, dissolution and API release to rationalise formulation design (Siepmann and Siepmann, 2013; Colombo et al.,

* Corresponding author.
E-mail address: jaz22@cam.ac.uk (J.A. Zeitler).
URL: http://thz.ceb.cam.ac.uk (J.A. Zeitler).

http://dx.doi.org/10.1016/j.ijpharm.2017.04.015

1995; Quodbach and Kleinebudde, 2016). In order to successfully predict tablet disintegration and API release, at least two mechanisms have to be considered: hydration kinetics, and the swelling of a tablet thereafter within complete release is achieved (Zuleger and Lippold, 2001; Narasimhan, 2001). It is important to note that the force necessary to break up the particle–particle bonds causing the disintegration of the tablet may also be generated by strain recovery (Desai et al., 2016; Quodbach and Kleinebudde, 2016; Markl and Zeitler, 2017). In contrast to the omni-directional enlargement of the swelling particles, strain recovery causes a uni-directional increase in size of the particles. The processes are interlinked and influenced strongly by the microstructure of the tablet. While a number of studies have investigated the effects on one of the mechanisms in isolation, only limited data are available on both. Absorption isotherms based on the weight of the samples during hydration were used to assess the extent of swelling (Schott, 1992b,a). It was observed that the rate of liquid uptake into their polymer matrix followed the same profile as the swelling; this indicates that both processes were controlled by the transport of the solvent into the polymer matrix (Schott, 1992b,a). Compacts of samples that contained a large amount of cross-linked polymer or micro-crystalline polymer both typically exhibit two subsequent phases of swelling: initial swelling due to liquid penetration and secondary swelling due to the disentanglement and diffusion of the polymers into the hydrating solution (Schott, 1992a,b).

In this work we demonstrate how mathematical models can be used to give detailed insight into liquid ingress and swelling dynamics. The model for the liquid ingress in a swelling tablet is based on Darcy's law and is compared to simulations using the well-known Washburn equation. The swelling is modelled by a Schott model, which was modified to enable the comparison with the experimental data and to describe the reduction in pore size. The models are calibrated and compared to experimental data from pure micro-crystalline cellulose (MCC) powder compacts measured by TPI during hydration in a flow cell.

2. Theory

2.1. Liquid penetration in a rigid porous medium

One of the key processes involved in the disintegration of a tablet is liquid penetration driven by capillary forces. Capillary transport is an important field of research due to its numerous applications, such as in petroleum engineering, in hydrology (e.g., movement of ground water), in consumer products (e.g., marker pens, candle wicks and sponges) or in plants (e.g., transport of water from the roots to the tips). The first analytical solution for capillary rise as a function of time was derived by Lucas and Washburn (1921). They described the flow through porous media by considering the pore space as a bundle of capillary tubes of varying diameter embedded in the solid matrix (see Fig. 1).

The location of the liquid front, L, across the entire porous medium can thus be expressed by the well-known Washburn equation as

$$L = \sqrt{R_e \frac{\gamma \cos\theta}{2\eta} t}, \tag{1}$$

where $R_e = R_h^2/R_{c,0}$ (with R_h as the hydraulic radius and $R_{c,0}$ as the pore radius of the dry material) is the mean effective pore radius, γ is the surface tension of the liquid, θ is the contact angle and η is the viscosity of the fluid.

Furthermore, the total volumetric flux of Newtonian liquids in an isotropic porous medium can be described by Darcy's law:

$$q = -\frac{K}{\eta}\frac{\Delta P}{L}. \tag{2}$$

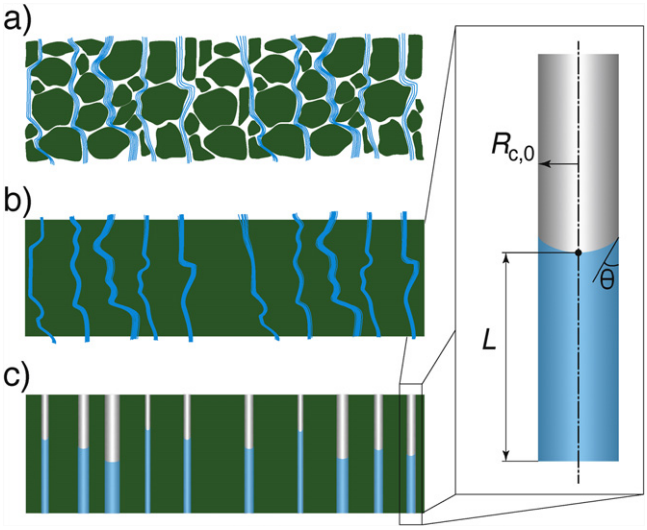

Fig. 1. Approximation of the porous structure of a powder compact. (a) The actual tablet consisting of forged particles forming channels through the powder compact. (b) Only the effective channels (with an effective pore size) are considered in the model. (c) Cylindrical channels are approximated from the pore structure. The inset highlights the capillary action in a cylindrical channel. Each channel is characterised by its liquid height L and its pore radius $R_{c,i}$ with an initial pore radius $R_{c,0}$. The contact angle θ is a fluid/matrix property which is assumed to be constant for all channels.

ΔP is the pressure difference and K is the intrinsic permeability, which is related to the properties of the porous pharmaceutical powder compact. The pressure difference can be described by the Young–Laplace equation ($\Delta P = P_c = \gamma\cos\theta/R_{c,0}$) considering only the capillary pressure, P_c, and neglecting the effect of gravity.

Assuming that the net mass flow in and out of the porous system must be zero (where inflows are negative and outflows are positive) in a rigid porous system, the continuity equation for incompressible fluids can be expressed as

$$\nabla q = 0. \tag{3}$$

In order to calculate $L(t)$ from Eq. (2) one needs to account for the fact that only a fraction of the volume is available for the liquid flow. Therefore, dividing q by ε_0 yields an equation for the liquid front depending on time in the form of

$$L = \sqrt{K \frac{4\gamma \cos\theta}{\varepsilon_0 \eta R_{c,0}} t}. \tag{4}$$

A detailed derivation of this equation was previously provided by Masoodi et al. (2007).

2.2. Liquid penetration in a swelling porous medium

Swelling of a porous medium causes a change in the intrinsic permeability, porosity and pore radius. Therefore, the aforementioned models are no longer valid and one has to consider the affect of swelling on liquid penetration. Schuchardt and Berg (1991) presented a model where they assumed a linear decrease with time of the pore radius in the wetted area of the porous medium (a composite of cellulose and superabsorbent fibres). They considered R_h as the effective hydrodynamic radius in the wetted region behind the advancing liquid front, which changes over time. $R_{c,0}$ is the capillary radius in the dry material and thus it is the length scale related to the liquid meniscus. R_h is approximated as a linear function of time by $R_h = R_{c,0} - a \cdot t$, where a is a constant and expresses the rate of

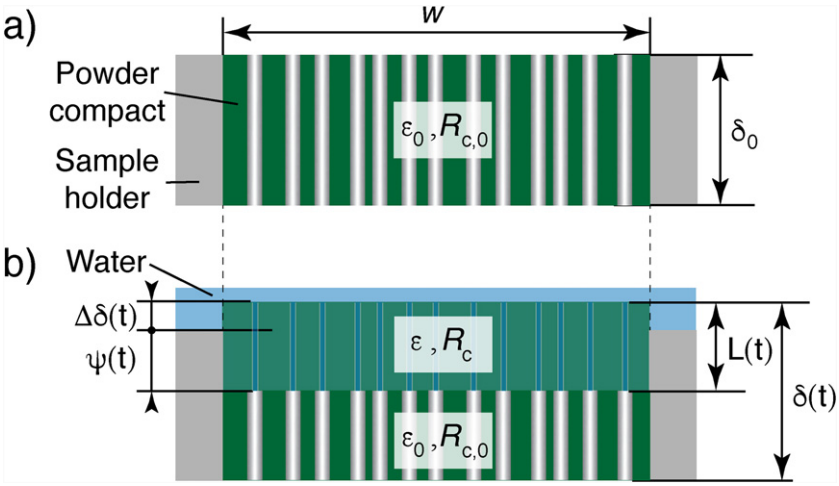

Fig. 2. Schematic of swelling and the ingress of fluid/solvent in the powder compact. The tablet is held tightly around its circumference by a sample holder. (a) Dry powder compact defining the initial tablet thickness δ_0, the tablet diameter w, the porosity ε_0 and the pore radius $R_{c,0}$. (b) Hydration of the powder compact by the dissolution medium. This defines the swelling $\Delta\delta$, displacement Ψ and the penetration depth $L = \Psi + \Delta\delta$. ε and R_c are the porosity and the pore radius of the wetted medium, respectively.

pore radius constriction. They used this assumption and modified the Washburn equation to give

$$L = \left(\frac{R_{c,0}\gamma\cos\theta}{2\eta}\right)^{1/2}\left(t - \frac{a}{R_{c,0}}t^2 + \frac{a^2}{3R_{c,0}^2}t^3\right)^{1/2}. \quad (5)$$

If the reduction rate constant $a = 0$, then Eq. (5) yields Eq. (1).

Masoodi and Pillai (2010) presented a model for the wicking and swelling of paper based on Darcy's law and under consideration of the dynamic change of porosity. Since swelling is an effect of liquid absorption by the polymer, the continuity equation as presented in Eq. (3) has to be modified to

$$\nabla q = -S - \frac{\partial\varepsilon}{\partial t}. \quad (6)$$

A negative term (i.e. sink term) on the right side of the equation corresponds to absorption of liquid by the matrix and thus it disappears from the pore space, whereas a positive term (i.e. source term) creates liquid in the pore space. S here is the rate of liquid absorption by the solid matrix and is positive for a swelling material. $\partial\varepsilon/\partial t$ is then negative as the porosity decreases in the wetted region. Masoodi and Pillai (2010) proposed a linear relation between S and the time derivative of the ratio between the solid and the total volume of the matrix. We further assume that the rate of increase of the dry particles' volume is equal to the volumetric rate of liquid absorption by solid matrix. This can be expressed as

$$S = \frac{\partial\varepsilon_s}{\partial t} = -\frac{\partial\varepsilon}{\partial t}, \quad (7)$$

using the relation between the porosity ε and the solid matrix ratio ε_s, i.e. $\varepsilon_s = 1 - \varepsilon$. The continuity equation then has the same form as Eq. (3). The model for liquid penetration in a swelling porous medium becomes

$$L = \sqrt{\frac{2P_c}{\varepsilon_0\eta}\int_0^t K(t')dt'}. \quad (8)$$

A detailed derivation of the model (henceforth referred to as modified Darcy's law approach) is given in Masoodi and Pillai (2010). The intrinsic permeability K changes with time. There are several established empirical and theoretical models in the literature for estimating the permeability. In this study we used a modified Carman–Kozeny equation with

$$K = D_s^2\frac{c}{180}\frac{\varepsilon^3}{(1-\varepsilon)^2}, \quad (9)$$

with D_s as the mean diameter of the powder particles. It is well-known that the Carman–Kozeny equation overestimates the permeability of porous beds (Rough et al., 2002), which is corrected for here by the constant c.

2.3. Modelling swelling pharmaceutical tablets

This section presents the new model to describe liquid ingress in swelling pharmaceutical tablets. The tablet is modelled as a cylinder with initial thickness δ_0 and diameter w. Due to the geometry of our experimental setup, where the sample is held tightly around its circumference (see Fig. 2), the tablet can only swell in the axial direction, causing an increase of the tablet thickness δ. Therefore, w and thus the cross-section area, A_t, of the tablet do not change during the hydration process. As in previous models, we also describe the pores as capillaries with initial radius $R_{c,0}$.

The tablet swells, increasing in height and causing the capillary radius, R_c, to decrease (Fig. 3). We propose that the fractional increase in volume of the wetted powder compact is equal to the

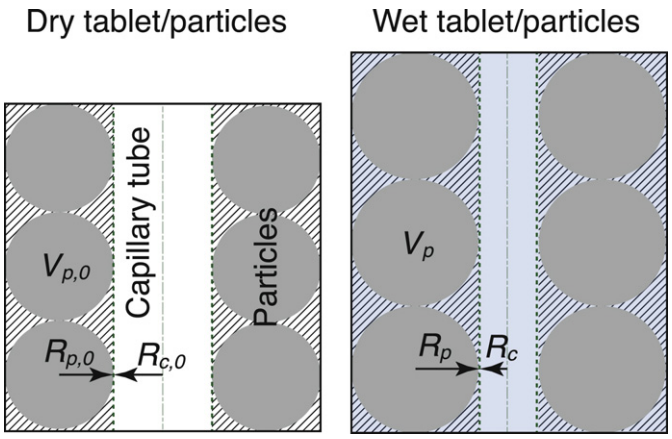

Fig. 3. Schematic of the swelling of the particles. The particle radius, R_p, directly impacts the capillary radius by $R_c = R_{c,0} - (R_p - R_{p,0})$. The striped and the grey areas are considered as the solid material in the presented model.

fractional increase in volume of a single wetted particle. Combining this assumption with $R_c = R_{c,0} - (R_p - R_{p,0})$ (see Fig. 3), the capillary radius can be expressed as a function of time as (the derivation is given in Appendix A). R_p and $R_{p,0} = D_{s/2}$ are the particle radius of the dry and wetted particle respectively

$$R_c = R_{c,0} - \frac{D_s}{2}\left[\left(\frac{\delta_0 + b \cdot t}{\delta_0}\right)^{1/3} - 1\right]. \quad (10)$$

Here b is the swelling rate, which can be determined using a swelling model as described below. The capillary tubes thus become constricted in the wetted region of the tablet (see Figs. 2 and 3).

The relative change in volume of the capillaries of a fully hydrated tablet can be expressed as

$$\frac{V_c}{V_{c,0}} = \frac{R_c^2 \pi \delta}{R_{c,0}^2 \pi \delta_0} = \frac{V_t}{V_{t,0}} \frac{R_c^2}{R_{c,0}^2}$$

with V_c and V_t as the capillary and the tablet volume in the wetted area and using $\delta = \frac{V_t}{V_{t,0}} \delta_0$. This can then be used to determine the porosity as a function of the capillary radius by

$$\varepsilon = \frac{V_c}{V_t} = \frac{V_{c,0} \frac{V_t}{V_{t,0}} \frac{R_c^2}{R_{c,0}^2}}{V_t} = \varepsilon_0 \frac{R_c^2}{R_{c,0}^2}. \quad (11)$$

The model describes the swelling process in terms of the constriction of the pores in the tablet matrix as they fill up with water during hydration. Once the pores are filled with water a stress is exerted on the solid bridges between the MCC particles by the pressure from the penetrating fluid. At the same time stored elastic potential energy that originates from the axial compaction is released when the MCC particles contact water. This relaxation process is relatively rapid (a time scale of seconds) and causes the particles to swell. Therefore, the swelling process induced by the liquid ingress is instantaneous and will last until the tablet is fully hydrated.

A second, much slower, phase of swelling follows the initial hydration if the tablet is still intact at this point, e.g. in formulations where no disintegrant is present. This second swelling process appears to be asymptotic in nature and can be modelled using the Schott model (Schott, 1992b,a), which was modified to (see Appendix B)

$$\Delta\delta = \frac{t}{\alpha + \frac{1}{\delta_\infty - \delta_0} t}. \quad (12)$$

α is a material constant that can be determined experimentally by linear regression and δ_∞ represents the maximum thickness of the tablet. α is related to the initial rate of swelling by

$$\lim_{t \to 0} \frac{d}{dt}(\Delta\delta) = \frac{1}{\alpha}. \quad (13)$$

We can replace b by $1/\alpha$ in Eq. (10). This represents the connection between the modified Schott model and the liquid penetration described by the modified Darcy's law approach. In line with the time used in Eq. (10), we defined $t = 0$ s when the tablet was exposed to the liquid.

Moreover, the swelling of the tablet provides a considerable amount of information regarding the strain that the tablet is undergoing during hydration. The resulting strain from tablet swelling is sometimes referred to as a swelling pressure (Bussemer et al., 2003). Understanding the mechanisms of swelling and how this impacts tablet disintegration allows formulators to assess the physical aspects of tablet disintegration and how the choice of excipients and their physical attributes (particle size, particle porosity, etc.) impacts disintegration. By fully understanding the mechanism of swelling in tablets, a rational design of the formulation with defined release kinetics of API can be achieved.

The main assumptions underlying the derivation of the presented models are:

1. The pore structure can be approximated by cylindrical tubes.
2. The absorption rate of liquid is equal to the (volumetric) swelling rate of the solid matrix.
3. The permeability is isotropic over the entire wetted area and it can be described by a modified Carman–Kozeny equation.
4. The porosity is uniform across the entire wetted volume.
5. The effect of gravity on liquid penetration is negligible.

Table 1
Properties of the powder compact and the solvent used in this study. Two different sets, labelled as F1 (3 repeats) and F2 (6 repeats), were prepared. The contact angle, θ, for MCC and water was taken from the literature (Steele et al., 2008).

		F1	F2
ε_0		0.10	0.15
D_s	μm	100	50
γ	N/mm	72.3	
δ_0	mm	1.50	
θ		64.3°	
η	mPa s	1.002	

3. Experimental

3.1. Materials and compression of tablet compacts

Flat-faced, round tablet compacts of 10 mm diameter were compressed using a compaction simulator (Phoenix Calibrations, Phoenix, AZ, USA). The device was instrumented to measure the forces of compaction throughout the compression cycle. Powder was loaded into the dies using a hopper and volumetric filling was performed to prepare two tablet sets with target porosities of $\varepsilon_0 = 0.10$ (labelled as F1; 3 repeats) and 0.15 (labelled as F2; 6 repeats) and a target thickness of 1.5 mm. The tablets used in this study were part of those presented in Yassin et al. (2015a). For this previous work the authors used only a subset of the prepared tablets. The compaction procedure and the porosities are the same. The porosity of two tablets of each set was measured by terahertz time-domain spectroscopy. It was also calculated from the volume of a tablet and the weighted average of the true density as well as by the tablet mass and the volume measured using helium pycnometry. The average porosities from the three methods were $10.45 \pm 0.30\%$ and $14.73 \pm 0.63\%$ for the 10% and 15% porosity tablets, respectively. The mean particle size differed, with $D_{s,F1} = 100$ μm and $D_{s,F2} = 50$ μm for F1 and F2, respectively. The samples consist of MCC using a grade which allowed direct compaction (Avicel® PH-102 for F1 and Avicel® PH-101 for F2, FMC BioPolymers, Philadelphia, PA, USA). The F2 tablets were only reported in the supporting information of Yassin et al. (2015a), and it is important to highlight that those tablets were produced using a different grade (Avicel® PH-101) than those presented in the main manuscript. The experiments were conducted with pure water as the liquid. The properties of the tablets and the liquid for each set are listed in Table 1.

3.2. Liquid penetration and swelling measurements using terahertz pulsed imaging (TPI)

A TPI Imaga 2000 (Teraview Ltd. Cambridge, UK) device coupled with a custom designed laminar flow cell was used to measure the disintegration process, as outlined previously (Yassin et al., 2015b). Signal processing techniques, including deconvolution using a double Gaussian filter and a simple averaging procedure, are used to

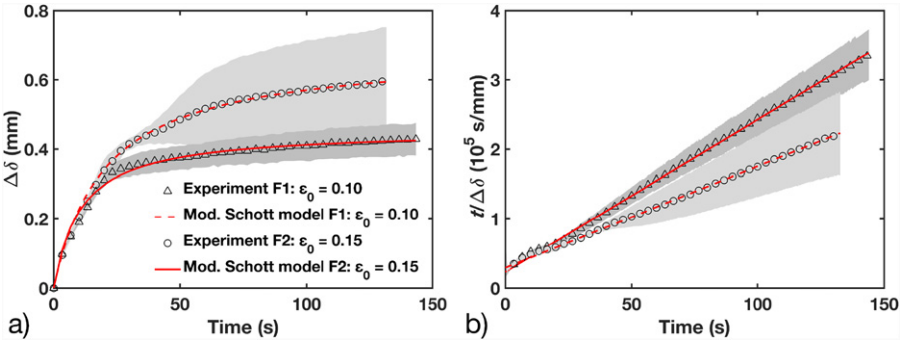

Fig. 4. Swelling behaviour of tablets plotted in (a) the swelling profile (every 5th data point is shown) and in (b) the linear representation of the modified Schott model (Eq. (12)). The average profiles of set F1 (black triangles) and of F2 (grey circles) were used to estimate α and δ_∞, which are required to simulate the modified Schott model (solid and dashed line). The shaded areas indicate the standard deviation calculated from the respective repeats.

remove noise and to enhance the features in the terahertz waveform (Yassin et al., 2015b; MacPherson, 2013; Zeitler and Shen, 2013).

The features observed in the deconvolved waveforms are due to the differences in refractive index between the different phases in the tablet during hydration: an initial peak (t_1) in the reflected time-domain waveform of the terahertz pulse originates from the tablet surface and is due to the difference between the refractive index of air ($n = 1$) and the tablet mixture (typically $1 < n < 2$). By tracking t_1 with time the swelling at the front surface of the tablet can be quantified. In the dry tablet the change in refractive index from the tablet material to air at the back surface of the tablet results in a negative response on the terahertz waveform (t_2) (Yassin et al., 2015a). Once the tablet comes into contact with water the t_2 response inverts into a positive peak due to the inherently higher refractive index of water ($n \approx 2.1$ at 1 THz and 20 °C) (Zelsmann, 1995) compared to air or polymer and this peak is referred to as t_3. By monitoring the position of t_3 with time it is possible to extract the velocity of the penetrating waterfront within the tablet. Consequently, these data allow the measurement of the swelling, $\Delta\delta$, and the displacement, Ψ, of the water front relative to the original tablet thickness δ_0 as illustrated in Fig. 2. The total liquid ingress in the porous medium, L, can then be calculated by $L = \Psi + \Delta\delta$.

4. Results and discussion

In the following section the experimental results will be compared to different mathematical models. Results for two different tablet sets (F1 and F2) are presented, which vary in terms of porosity ($\varepsilon_{0,F1} = 0.10$ and $\varepsilon_{0,F2} = 0.15$) and mean particle size ($D_{s,F1} = 100\,\mu m$ and $D_{s,F2} = 50\,\mu m$). By relating the TPI measurements to models of swelling and liquid ingress we gain a better understanding of the physical transformations that occur within the tablet. This discussion will be split into two sections: (1) application of the modified Schott model to describe tablet swelling, and (2) application of the Darcy approach to model the liquid penetration of swelling porous media.

4.1. Application of the modified Schott model

As outlined above, the Schott model describes a swelling process that results from the unravelling of the polymer macromolecules after diffusion into solvent upon hydration (Schott, 1992a). To determine the parameters α and δ_∞ it is most convenient to rearrange Eq. (12) in a linear form $t/\Delta\delta = \alpha + t/(\delta_\infty - \delta_0)$, where A and $1/(\delta_\infty - \delta_0)$ can be extracted from the y intercept and the gradient of the linear fit, respectively (Fig. 4). During extraction of the α and δ_∞ parameters care is taken to restrict the fit to the data where no cracks form in the tablet as this significantly affects the swelling behaviour. The parameters obtained are listed in Table 2. A clear difference between the two data sets is evident. The tablet sets with a higher porosity and smaller particle size swell more towards the end of the experiment, as indicated by a smaller gradient (see Fig. 4). Using the values of α and δ_∞ it is possible to compare the swelling behaviour of individual tablets and the average swelling profile (Fig. 5). The Schott model approximates the swelling behaviour quite well (adjusted $R^2 = 0.999$ and $R^2 = 0.998$ for F1 and F2, respectively), but it does not follow the experimental swelling results of individual samples perfectly. This is attributed to the inherent variations in the tablet microstructure after compaction.

The swelling profiles that were measured by TPI from these samples can be separated into two phases of swelling, the transition between which is indicated by the vertical dashed line in Fig. 5. The transition time of the two phases was chosen as the time when the swelling rate dropped significantly, which is approximately the time when the tablet was fully hydrated. The first phase of swelling is dominated by fluid ingress into the dry tablet matrix. Once the initial liquid penetration ceases the rate of swelling decreases. All three profiles show that the magnitude of swelling in the second phase is less than in the first phase ($\Delta\delta = 0.3$ mm vs. $\Delta\delta = 0.1$ mm). The reason why we observe the first phase of penetration induced swelling in such a pronounced way can be attributed to the hygroscopicity of MCC. As a result liquid penetration is facilitated and hence there will be a sharp change in capillary pressure as water begins to fill the pores.

The last data point of the liquid ingress, Ψ, measured by TPI occurs between 1.2 and 1.4 mm, which indicates that the water front had almost reached the front face of the tablet. However, the reason that we cannot resolve the final stage of the hydration process is twofold: (i) due to the optics (i.e. the focus was set to the centre of the tablet) and the resolution limit of the terahertz system used; (ii) due to spreading of the liquid with increasing penetration depth causing an indistinct liquid front. Therefore, the peaks in the terahertz waveform originating from the water front, t_3, and from the front face of the tablet, t_1, cannot be differentiated at this point.

None of the tablets disintegrated and therefore there is no contribution from fracture to the swelling process. Fracture may be observed in MCC tablets with a larger porosity, where fractures form within the tablet matrix. However, in a number of immediate release formulations swelling is controlled by the penetration of the solvent through the tablet matrix alone as the tablet already starts to disintegrate before the secondary swelling stage is reached. This is often the case for tablets that do not contain a binder and samples that contain a mixture of MCC and a superdisintegrant (Yassin et al., 2015a).

Table 2
Material parameters for the two different tablet sets F1 ($\varepsilon_0 = 0.10$) and F2 ($\varepsilon_0 = 0.15$). A and δ_∞ are parameters for the modified Schott model. The scaling parameter c for the permeability and the pore radius $R_{c,0}$ were estimated from the data set of F1 and $R_{c,0}$ was adapted for F2 tablets using Eq. (15). The modified Darcy's law approach was applied to calculate the liquid ingress for the F2 tablets and therefore, the parameters of the other models were not calculated. The parameter c was estimated using the mod. Darcy's law approach. The same value was used for the Darcy's law approach. The standard deviations were calculated from the 95% confidence interval of each parameter.

		F1	F2
α	s/mm	23.321 ± 0.006	29.359 ± 0.433
δ_∞	mm	1.956 ± 0.001	2.235 ± 0.003
c (Darcy's law approach)	-	0.17 ± 0.04	-
c (mod. Darcy's law approach)	-	0.17 ± 0.04	0.17± 0.04
R_e (Washburn eq.)	nm	9.8 ± 0.2	-
$R_{c,0}$ (Darcy's law approach)	μm	95.2 ± 1.8	-
$R_{c,0}$ (mod. Darcy's law approach)	μm	75.7 ± 24.2	92.7 ± 29.6

4.2. Liquid penetration in a swelling porous medium

The liquid ingress was described by the Washburn equation (Eq. (1)), the Darcy law approach (Eq. (4)) and the modified Darcy law approach (Eq. (8)). The Washburn equation requires an estimate of the effective pore radius R_e and for the other two models we have to know the initial pore radius, $R_{c,0}$, and the scaling factor c for the permeability. The values of R_e, $R_{c,0}$ and c were fitted using the average liquid ingress profile of the F1 tablets. Fig. 6 compares the simulation results using the different models to the experimental data measured by TPI. It is important to note that the Washburn and Darcy's law approaches yield the same penetration kinetics due to their similarity and the fitting of the parameters.

In order to use the model for the prediction of F2 samples, we have to adapt the pore radius. We propose to adapt $R_{c,0}$ based on the porosity ratio (area-based porosity) between the two different sets

$$\frac{\varepsilon_{0,F1}}{\varepsilon_{0,F2}} = \frac{N_{F1}R_{c,0,F1}^2\pi/A_t}{N_{F2}R_{c,0,F2}^2\pi/A_t} = \frac{N_{F1}R_{c,0,F1}^2}{N_{F2}R_{c,0,F2}^2}, \tag{14}$$

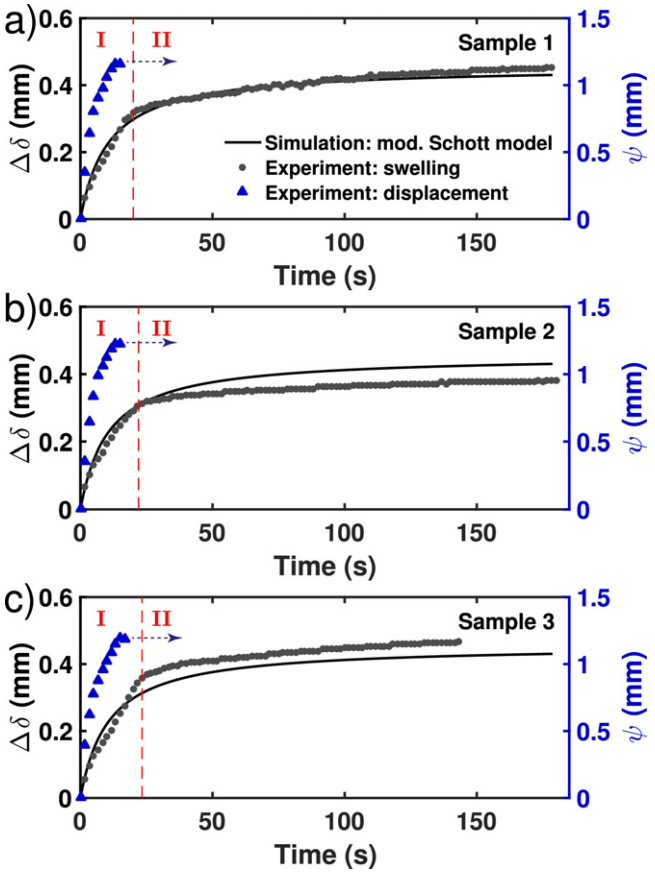

Fig. 5. Comparison of tablet swelling in individual tablets analysed using TPI (black circles) and calculated swelling using the Schott model (solid lines) where (a), (b) and (c) are experimental repeats of tablets of F1. The solid points are experimental data and the solid lines are the results using the model generated from the average swelling profile of all three samples. The blue triangles represent the liquid ingress, Ψ, measured using the TPI by tracking the t_3 peak of the time-domain waveform. The dashed vertical red line marks the transition from penetration controlled swelling (stage I) to polymer absorption controlled swelling (stage II), when the dry matrix is fully hydrated. (For interpretation of the references to colour in this figure legend, the reader is referred to the web version of the article.)

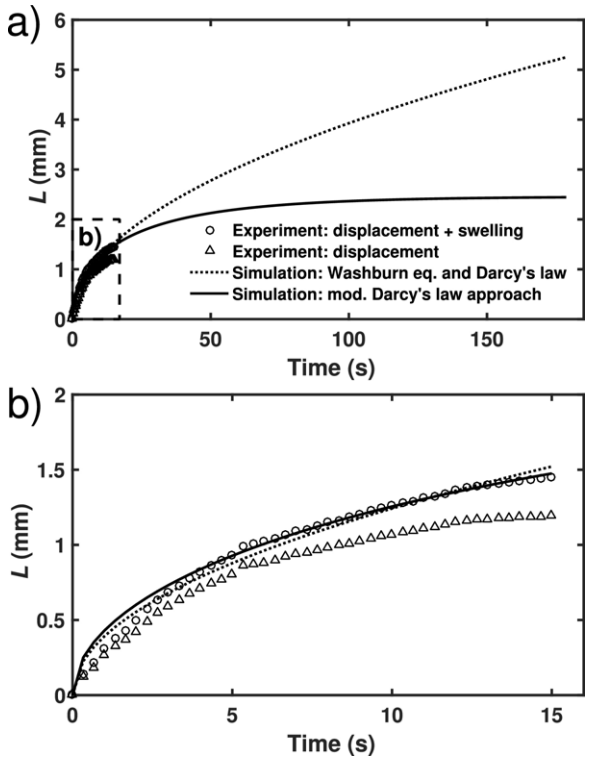

Fig. 6. Simulation results and experimental data of liquid penetration for average displacement and swelling of tablet set F1. Simulations were performed for the entire experimental time as shown in (a). However, the displacement could only be measured for the first 15 s of the experiment, as depicted in (b). The dotted line is the simulation result using the Washburn equation (Eq. (1)) and Darcy's law approach (Eq. (4)). Due to the fitting and the similarity of the Washburn equation (Eq. (1)) and the Darcy's law approach (Eq. (4)), both models yield the same results (dotted line). The solid line corresponds to the modified Darcy's law approach (Eq. (8)) considering swelling and the dynamic change of porosity. The grey triangles represent the displacement, Ψ, measured using the TPI by tracking the t_3 peak of the time-domain waveform and the solid circles depict the liquid ingress, $L = \Psi + \Delta\delta$, with the swelling $\Delta\delta$ measured using TPI (tracking of the t_1 peak in the terahertz waveform).

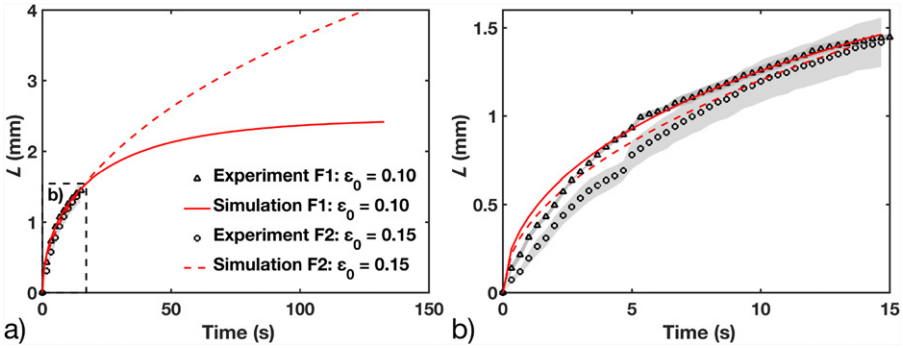

Fig. 7. Liquid ingress of F1 (black triangles) and F2 (grey solid circles) samples together with the respective simulations (solid and dashed line) using the modified Darcy's law approach (Eq. (8)). (a) shows the simulation for the entire experimental time and (b) provides further detail of the initial hydration phase.

N_{F1} and N_{F2} are the number of capillaries in sample F1 and F2 respectively. We can derive an equation for the pore radius of tablet set F2 as a function of the porosities, the number of pores, and the pore radius of tablet set F1:

$$R_{c,0,F2} = \left(\frac{N_{F2}}{N_{F1}}\frac{\varepsilon_{0,F2}}{\varepsilon_{0,F1}}\right)^{1/2} R_{c,0,F1} \tag{15}$$

We estimated the ratio of the number of capillaries from the ratio of the number of particles in F1 and F2. The number of particles, N_p, can be approximated by $N_p = A_t/(R_p^2\pi)$ with $R_p = D_s/2$. The ratio of the number of capillaries in F1 and in F2 can thus be expressed as $N_{F2}/N_{F1} = N_{p,F2}/N_{p,F1} = R_{p,F1}^2/R_{p,F2}^2 = 4$. Eq. (15) can be applied to a sample with a different porosity than that used for the fitting. Consequently, the parameters required for the Darcy's law approach were estimated from the data from the F1 tablets. The pore radius was adapted for the F2 tablets based on Eq. (15), whereas c was kept constant for all samples. The parameters are summarised in Table 2. Interestingly the onset of liquid ingress is faster for the F1 powder compacts (Fig. 7). This can be attributed to the larger particle size of the tablet set F1, which cause a larger swelling in the initial phase. However, the total swelling is larger for the smaller particles (δ_∞ is 1.96 mm and 2.23 mm for F1 and F2 tablets and see Fig. 4) and thus the liquid can penetrate considerably further into the powder compact.

It is interesting to note that there is a consistent discrepancy between the swelling model and the experimental data in the initial 2 s. The model predicts a faster onset of swelling compared to that we observed using TPI. We believe that this is due to the experimental setup: at the beginning of the experiment the flow cell is filled with liquid from bottom to top and thus the tablet is also wetted from bottom to top. Therefore, it takes a few seconds for the entire tablet face to be wetted, which slows down the initial liquid ingress. Improvement of the experimental setup is the subject of further research.

There is only a slight difference between the Washburn equation/Darcy's law and the modified Darcy's law approach at the beginning of the experiment, whereas they differ noticeably and the experimental data towards the end. This is not surprising as the Washburn equation and the Darcy's law approach do not consider any change in porosity which leads to a constant pressure and constant permeability. The performance of the models can be quantified for the F1 tablets by the adjusted R^2, which is 0.994 and 0.982 for the mod. Darcy's law approach and the Washburn equation/Darcy's law, respectively. The liquid penetration for short time-scales depends linearly on the time and thus it deviates from the $\sqrt{t}$ behaviour as assumed in the Washburn equation and in both Darcy's law approaches. Such kinetics were previously discussed by Ridgway and Gane (2002), where the liquid absorption changed from an inertial Bosanquet regime ($L \propto t$) to the viscous Laplace–Poiseuille flow regime ($L \propto \sqrt{t}$). Therefore, the performance of the models for short-time scales may be improved by considering the Bosanquet regime. There is also the effect of the initial acceleration associated with the formation of the meniscus, which the Washburn equation does not consider.

Moreover, the porosity, pore radius and permeability undergo a significant change as highlighted in Fig. 8. It is clear that the average pore radius decreases as the individual particle swells, which causes a decrease of the porosity. As the permeability is also a function of the pore radius, it changes over time as well. The dynamic changes are less pronounced for the tablet set with the larger porosity ($\varepsilon_0 = 0.15$), which is primarily due to the smaller particle size of the MCC particles. The number of particles compacted is larger for smaller particles in order to reach the same tablet solid fraction as

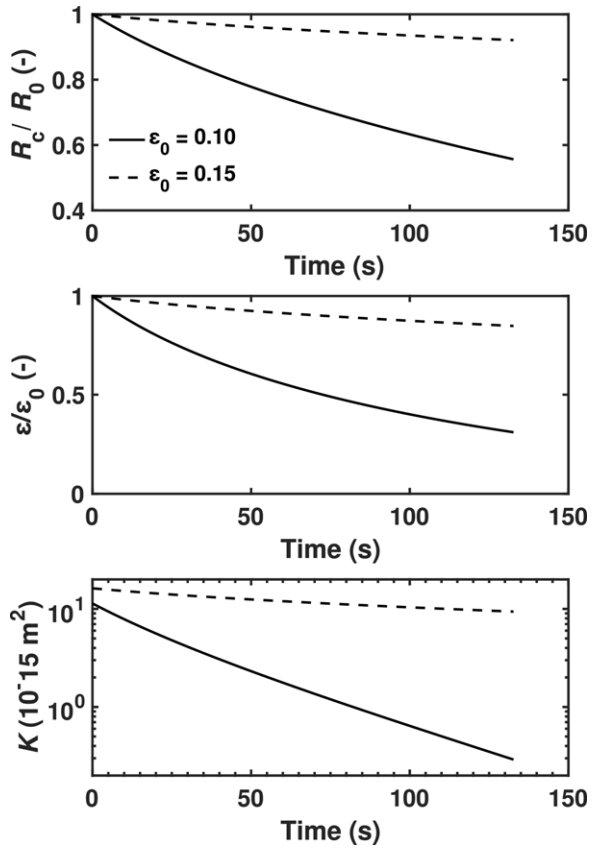

Fig. 8. Simulation results using the modified Darcy's law approach of pore radius ratio, porosity ratio and permeability for the two different tablet sets, F1 ($\varepsilon_0 = 0.10$, solid line) and F2 ($\varepsilon_0 = 0.15$, dashed line). $R_{c,0}$ (ε_0) is the initial pore radius (porosity) and R_c (ε) is the pore radius (porosity) at time t.

when using larger particles. Therefore, both the porosity and the particle size have to be considered for the interpretation, whereas the impact of the particle size is slightly more significant in this case due to the larger relative difference in particle size between the two tablet sets compared to that for the porosity. The relative differences, *RD*, were calculated by $RD = |x_{F1} - x_{F2}|/(x_{F1} + x_{F2})$ with x as the particle size or the porosity and with the subscript indicating the tablet set. The *RD* in particle size and in porosity were 0.33 (=|100 μm − 50 μm|)/150 μm) and 0.20 (=|0.10 − 0.15|/0.25). Since the total amount of swelling is similar for the two tablet sets, the swelling rate of each single particle is smaller for F2 than for F1 tablets, which leads to a slower decrease of the capillary tube radius of the F2 tablets. However, the larger initial porosity of F2 samples causes a larger initial permeability compared to the permeability of F1 tablets.

The results for F1 and F2 (Fig. 8) highlight that the permeability is sensitive to the microstructure of the tablets. One additional factor which is expected to play a significant role is the formation of (micro) cracks within the tablets during disintegration and the subsequent crack propagation during swelling. This results in the build up of considerable strain in the particle matrix. The strain is the driving force for crack formation in the tablet structure and once a crack has formed the porosity within the tablet matrix increases. As a result liquid penetration is facilitated, the tablet swells further and the crack propagates through the matrix driven by the additional swelling of the matrix. There were no noticeable discontinuities in the experimental data which would indicate the presence of macroscopic cracks.

5. Conclusions

We have shown that it is possible to describe the liquid ingress and the swelling in powder compacts using mathematical models. By applying these models it is possible to gain insights into the mechanism of liquid ingress and swelling in tablets upon hydration. The models further allow the analysis of the reduction of pore radius, dynamic changes in porosity as well as in permeability.

The drawback of the mathematical model described in this study is that it combines a theoretical model with an empirically derived model (the modified Schott model) and therefore relies on having to calibrate for A and δ_∞ prior to using the model for predictions. It would be highly desirable to develop models based on the physical properties of the powder and dry tablets alone. Such a model would reduce the amount of work needed to understand the impact of subtle changes in formulation on the product performance. The presented model does not take into account fracture controlled swelling, which may play an important role during disintegration of other formulations. More research is necessary to describe the formation and propagation of cracks and its impact on the disintegration.

Moreover, the models presented in this study require an average pore radius, which was estimated from experimental data. In future key characteristics of the microstructure, such as the pore radius, of porous powder compacts can be measured using X-ray computed microtomography (Al-Raoush and Willson, 2005) or a nitrogen adsorption method (Westermarck et al., 1999). It could be calculated by a theoretical model based on the particle size distribution (Nordström et al., 2013). This will, however, require the development of a relation between a measured pore radius or pore size distribution and the effective pore size driving the liquid ingress. Every methodology used to measure the pore size as well as the porosity has to be critically assessed as the results from different methods might differ considerably depending on the underlying physical measurement principle. Furthermore, the presented models describe the microstructure only by the porosity and an average pore radius and do not consider parameters like tortuosity, connectivity of pores, constriction of pores or pore size distribution (inter- and intra-granular pores) (Berg, 2014). Therefore, there is potential to increase the accuracy and generality of the models and to eventually provide models which can be used for formulation development.

Acknowledgements

We would like to thank GlaxoSmithKline for allowing us to use their compaction simulator, providing us with excipient materials, and sharing their valuable experience and advice. We are very grateful to Juraj Sibik for valuable discussions and suggestions. D.M. and J.A.Z. would like to acknowledge the U.K. Engineering and Physical Sciences Research Council (EPSRC) for funding (EP/L019922/1). S.Y. would like to thank the EPSRC for a studentship. Additional data related to this publication are available at the Cambridge University repository (https://doi.org/10.17863/CAM.9101).

Appendix A. Pore radius reduction

The volume ratio for a wetted tablet is given by

$$\frac{V_t}{V_{t,0}} = \frac{\delta(t)A_t}{\delta_0 A_t} = \frac{\delta_0 + b \cdot t}{\delta_0} \tag{A.1}$$

and for a single wetted particle

$$\frac{V_p}{V_{p,0}} = \frac{\frac{3}{4}\pi R_p^3}{\frac{3}{4}\pi R_p^3} = \frac{R_p^3}{R_{p,0}^3}, \tag{A.2}$$

where A_t is the surface area of the tablet, R_p is the particle radius at time t, $R_{p,0} = D_s/2$ is the initial particle radius, and b is the swelling rate. The tablet can only swell in its axial direction as it is tightly held around its circumference. The swelling of an individual particle can swell in all 3 directions causing the reduction of the capillary tube radius. Although the particles at the tablet band will be restricted by the sample holder to swell in the radial direction, this will have a negligible impact on the swelling behaviour of the particles at the tablet centre where we performed the TPI measurements. Using Eqs. (A.1) and (A.2) we can derive an expression for the change of the wetted particle radius as a function of time:

$$\begin{aligned} \frac{R_p^3}{(D_s/2)^3} &= \frac{\delta_0 + b \cdot t}{\delta_0} \\ R_p &= \left(\frac{\delta_0 + b \cdot t}{\delta_0}\right)^{1/3} \frac{D_s}{2} \end{aligned} \tag{A.3}$$

An increase of the particle radius causes a decrease of the capillary radius:

$$\begin{aligned} R_c &= R_{c,0} - \left(R_p - \frac{D_s}{2}\right) \\ &= R_{c,0} - \frac{D_s}{2}\left[\left(\frac{\delta_0 + b \cdot t}{\delta_0}\right)^{1/3} - 1\right]. \end{aligned} \tag{A.4}$$

Alternatively to the simple linear relationship between the particle radius and the capillary radius, we could assume that the total

cross-section area of the particles plus the area of the capillaries is constant. This can be expressed by

$$\begin{aligned} N_p R_p^2 + N R_c^2 &= N_p R_{p,0}^2 + N R_{c,0}^2 \\ N R_c^2 &= N_p R_{p,0}^2 + N R_{c,0}^2 - N_p R_p^2 \\ N R_c^2 &= N_p \left(R_{p,0}^2 - R_p^2\right) + N R_{c,0}^2 \end{aligned} \tag{A.5}$$

$$R_c^2 - R_{c,0}^2 = \frac{N_p}{N}\left(R_{p,0}^2 - R_p^2\right),$$

where N_p is the number of particles per unit area and N is the number of capillary tubes. This leads to the following expression for the capillary radius as a function of the particle size

$$\begin{aligned} R_c &= \sqrt{R_{c,0}^2 + \frac{N_p}{N}\left[R_{p,0}^2 - R_p^2\right]} \\ &= \sqrt{R_{c,0}^2 - \frac{N_p}{N}\left(\frac{D_s}{2}\right)^2\left[\left(\frac{\delta_0 + b\cdot t}{\delta_0}\right)^{2/3} - 1\right]}. \end{aligned} \tag{A.6}$$

Since Eq. (A.6) introduces another fitting parameter (N_p/N), we used Eq. (A.4) in this study.

Appendix B. Modified Schott model

The Schott model represented as a second-order equation is defined as

$$\frac{dW}{dt} = k(W_\infty - W)^2 \tag{B.1}$$

with W the liquid uptake in gram of solution per gram of medium at time t, W_∞ the maximum or equilibrium uptake and k a constant. Solving Eq. (B.1) yields the water uptake dependency on time:

$$W = \frac{t}{\alpha + \frac{t}{W_\infty}} \tag{B.2}$$

$\alpha = 1/(kW_\infty)$ is a constant and corresponds to the reciprocal of the initial swelling rate. In order to apply this model to the one dimensional swelling case in this study, we need to substitute W and W_∞:

$$W = \frac{A_t \Delta\delta \rho_l}{A_t \delta_0 \rho_s} = \frac{\Delta\delta}{\delta_0}\frac{\rho_l}{\rho_s} \tag{B.3}$$

$$W_\infty = \frac{A_t(\delta_\infty - \delta_0)\rho_l}{A_t \delta_0 \rho_s} = \frac{\delta_\infty - \delta_0}{\delta_0}\frac{\rho_l}{\rho_s} \tag{B.4}$$

$\Delta\delta$ is the extent of swelling and is given by

$$\Delta\delta = \delta - \delta_0. \tag{B.5}$$

A_t is the surface area of the tablet face. ρ_l and ρ_s are the densities of the liquid and the solid matrix, respectively. δ_∞ is the maximum or equilibrium thickness of the tablet, which is related to the maximum liquid uptake W_∞. Combining Eqs. (B.1), (B.3) and (B.4), yields

$$\begin{aligned} \frac{1}{\delta_0}\frac{\rho_l}{\rho_s}\frac{d\Delta\delta}{dt} &= k\left(\frac{\delta_\infty - \delta_0}{\delta_0}\frac{\rho_l}{\rho_s} - \frac{\Delta\delta}{\delta_0}\frac{\rho_l}{\rho_s}\right)^2 \\ \Delta\delta &= \frac{k(\delta_\infty - \delta_0)^2 \frac{\rho_l}{\rho_s} t}{k(\delta_\infty - \delta_0)\frac{\rho_l}{\rho_s} t + \delta_0} \end{aligned} \tag{B.6}$$

Eq. (B.6) can be written in the form of the Schott model (Eq. (B.2)) by defining

$$k = \frac{\delta_0}{(\delta_\infty - \delta_0)^2 \alpha}\frac{\rho_s}{\rho_l}. \tag{B.7}$$

The modified Schott model is then

$$\Delta\delta = \frac{\frac{\delta_0}{\alpha}t}{\delta_0 + \frac{\delta_0}{\alpha(\delta_\infty - \delta_0)}t} = \frac{t}{\alpha + \frac{1}{\delta_\infty - \delta_0}t} \tag{B.8}$$

References

Al-Raoush, R.I., Willson, C.S., 2005. Extraction of physically realistic pore network properties from three-dimensional synchrotron X-ray microtomography images of unconsolidated porous media systems. J. Hydrol. 300, 44–64.

Battu, S.K., Repka, M.A., Majumdar, S., Rao, Y.M., 2007. Formulation and evaluation of rapidly disintegrating fenoverine tablets: effect of superdisintegrants. Drug Dev. Ind. Pharm. 33, 1225–1232.

Berg, C.F., 2014. Permeability description by characteristic length, tortuosity, constriction and porosity. Transp. Porous Media 103, 381–400.

Bi, Y.X., Sunada, H., Yonezawa, Y., Danjo, K., 1999. Evaluation of rapidly disintegrating tablets prepared by a direct compression method. Drug Dev. Ind. Pharm. 25, 571–581.

Bussemer, T., Peppas, N.A., Bodmeier, R., 2003. Evaluation of the swelling, hydration and rupturing properties of the swelling layer of a rupturable pulsatile drug delivery system. Eur. J. Pharm. Biopharm. 56, 261–270.

Chen, Y.Y., Hughes, L.P., Gladden, L.F., Mantle, M.D., 2010. Quantitative ultra-fast MRI of HPMC swelling and dissolution. J. Pharm. Sci. 99, 3462–3472.

Colombo, P., Bettini, R., Massimo, G., Catellani, P.L., Santi, P., Peppas, N.A., 1995. Drug diffusion front movement is important in drug release control from swellable matrix tablets. J. Pharm. Sci. 84, 991–997.

Corveleyn, S., Remon, J.P., 1997. Formulation and production of rapidly disintegrating tablets by lyophilisation using hydrochlorothiazide as a model drug. Int. J. Pharm. 152, 215–225.

Davis, S.S., Hardy, J.G., Fara, J.W., 1986. Transit of pharmaceutical dosage forms through the small intestine. Gut 27, 886–892.

Desai, P.M., Liew, C.V., Heng, P.W.S., 2016. Review of disintegrants and the disintegration phenomena. J. Pharm. Sci. 105, 2545–2555.

Fyfe, C.A., Blazek, A.I., 1997. Investigation of hydrogel formation from hydroxypropylmethylcellulose (HPMC) by NMR spectroscopy and NMR imaging techniques. Macromolecules 30, 6230–6237.

Gupta, E., Barends, D.M., Yamashita, E., Lentz, K.A., Harmsze, A.M., Shah, V.P., Dressman, J.B., Lipper, R.A., 2006. Review of global regulations concerning biowaivers for immediate release solid oral dosage forms. Eur. J. Pharm. Sci. 29, 315–324.

Kazarian, S., van der Weerd, J., 2008. Simultaneous FTIR spectroscopic imaging and visible photography to monitor tablet dissolution and drug release. Pharm. Res. 25, 853–860.

Kazarian, S.G., Chan, K.L.A., 2006. Applications of ATR-FTIR spectroscopic imaging to biomedical samples. Biochim. Biophys. Acta 1758, 858–867.

Lin, S.Y., 1988. Effect of excipients on tablet properties and dissolution behavior of theophylline-tableted microcapsules under different compression forces. J. Pharm. Sci. 77, 229–232.

MacPherson, E., 2013. Biomedical Imaging. Volume 171 of Springer Series in Optical Sciences, Springer, Berlin/Heidelberg, pp. 415–431 (Chapter 16).

Markl, D., Zeitler, J.A., 2017. A review of disintegration mechanisms and measurement techniques. Pharm. Res., 1–28, http://dx.doi.org/10.1007/s11095-017-2129-z.

Masoodi, R., Pillai, K.M., 2010. Darcy's law-based model for wicking in paper-like swelling porous media. AIChE J. 56, 2257–2267.

Masoodi, R., Pillai, K.M., Varanasi, P.P., 2007. Darcy's law-based models for liquid absorption in polymer wicks. AIChE J. 53, 2769–2782.

Narasimhan, B., 2001. Mathematical models describing polymer dissolution: consequences for drug delivery. Adv. Drug Deliv. Rev. 48, 195–210.

Nordström, J., Persson, A.S., Lazorova, L., Frenning, G., Alderborn, G., 2013. The degree of compression of spherical granular solids controls the evolution of microstructure and bond probability during compaction. Int. J. Pharm. 442, 3–12.

Quodbach, J., Kleinebudde, P., 2016. A critical review on tablet disintegration. Pharm. Dev. Technol. 21, 763–774.

Rajabi-Siahboomi, A., Bowtell, R., Mansfield, P., Davies, M., Melia, C., 1996. Structure and behavior in hydrophilic matrix sustained release dosage forms: 4. Studies of water mobility and diffusion coefficients in the gel layer of HPMC tablets using NMR imaging. Pharm. Res. 13, 376–380.

Rajabi-Siahboomi, A.R., Bowtell, R.W., Mansfield, P., Henderson, A., Davies, M.C., Melia, C.D., 1994. Structure and behaviour in hydrophilic matrix sustained release dosage forms: 2. NMR-imaging studies of dimensional changes in the gel layer and core of HPMC tablets undergoing hydration. J. Control. Release 31, 121–128.

Ridgway, C.J., Gane, P.A.C., 2002. Dynamic absorption into simulated porous structures. Colloids Surf. A: Physicochem. Eng. Asp. 206, 217–239.

Rough, S.L., Bridgwater, J., Wilson, D.I., 2002. In situ measurements of porosities and permeabilities of alumina pastes. Powder Technol. 123, 262–274.

Sarantopoulos, P.D., Altiok, T., Elsayed, E.A., 1995. Manufacturing in the pharmaceutical industry. J. Manuf. Syst. 14, 452–467.

Schott, H., 1992a. Kinetics of swelling of polymers and their gels. J. Pharm. Sci. 81, 467–470.

Schott, H., 1992b. Swelling kinetics of polymers. J. Macromol. Sci. B 31, 1–9.

Schuchardt, D.R., Berg, J.C., 1991. Liquid transport in composite cellulose – superabsorbent fiber networks. Wood Fiber Sci. 23, 342–357.

Segale, L., Giovannelli, L., Pattarino, F., Conti, S., Maggi, L., Grenier, P., Vergnault, G., 2010. Thermogravimetric investigation of the hydration behaviour of hydrophilic matrices. J. Pharm. Sci. 99, 2070–2079.

Siepmann, J., Siepmann, F., 2013. Mathematical modeling of drug dissolution. Int. J. Pharm. 453, 12–24.

Steele, D.F., Moreton, R.C., Staniforth, J.N., Young, P.M., Tobyn, M.J., Edge, S., 2008. Surface energy of microcrystalline cellulose determined by capillary intrusion and inverse gas chromatography. AAPS J. 10, 494–503.

Washburn, E.W., 1921. The dynamics of capillary flow. Phys. Rev. 17, 273–283.

Westermarck, S., Juppo, A.M., Kervinen, L., Yliruusi, J., 1999. Microcrystalline cellulose and its microstructure in pharmaceutical processing. Eur. J. Pharm. Biopharm. 48, 199–206.

Yassin, S., Goodwin, D.J., Anderson, A., Sibik, J., Wilson, D.I., Gladden, L.F., Zeitler, J.A., 2015a. The disintegration process in microcrystalline cellulose based tablets, part 1: influence of temperature, porosity and superdisintegrants. J. Pharm. Sci. 104, 3440–3450.

Yassin, S., Su, K., Lin, H., Gladden, L.F., Zeitler, J.A., 2015b. Diffusion and swelling measurements in pharmaceutical powder compacts using terahertz pulsed imaging. J. Pharm. Sci. 104, 1658–1667.

Yu, L., 2008. Pharmaceutical quality by design: product and process development, understanding, and control. Pharm. Res. 25, 781–791.

Zeitler, J.A., Shen, Y.C., 2013. Industrial Applications of Terahertz Imaging. Volume 171 of Springer Series in Optical Sciences, Springer, Berlin/Heidelberg, pp. 451–489 (Chapter 18).

Zelsmann, H.R., 1995. Temperature dependence of the optical constants for liquid H_2O and D_2O in the far IR region. J. Mol. Struct. 350, 95–114, http://dx.doi.org/10.1016/0022-2860(94)08471-S.

Zhang, Q., Gladden, L., Avalle, P., Mantle, M., 2011. In vitro quantitative 1H and 19F nuclear magnetic resonance spectroscopy and imaging studies of Fluvastatin™ in Lescol XL® xl tablets in a USP-IV dissolution cell. J. Control. Release 156, 345–354.

Zhang, Q., Gladden, L.F., Avalle, P., Zeitler, J.A., Mantle, M.D., 2013. Terahertz pulsed imaging and magnetic resonance imaging as tools to probe formulation stability. Pharmaceutics 5, 591–608.

Zuleger, S., Lippold, B.C., 2001. Polymer particle erosion controlling drug release. I. Factors influencing drug release and characterization of the release mechanism. Int. J. Pharm. 217, 139–152.